Available online at www.sciencedirect.com
ScienceDirect
Electrochimica Acta 52 (2007) 4182–4190
ELECTROCHIMICA Acta
www.elsevier.com/locate/electacta

Finely dispersed Pt nanoparticles in conducting poly(*o*-anisidine) nanofibrillar matrix as electrocatalytic material

C. Sivakumar *

Electrodics & Electrocatalysis Division, Central Electrochemical Research Institute, Karaikudi 630006, Tamil Nadu, India

Received 2 July 2006; received in revised form 23 November 2006; accepted 27 November 2006
Available online 12 January 2007

Abstract

A new approach based on stepwise oxidation of *o*-anisidine is explored for generating nanoporous films of poly(*o*-anisidine), POA and loading of Pt nanoparticles that are subsequently used for electrocatalysis of methanol oxidation are presented and compared with bulk Pt. POA film can easily be prepared by stepwise electro-oxidation procedure with very high porosity consisting of nanofibrillar structure using without templates. Controlled sizes of Pt nanoparticles were entrapped into POA matrix by a two-step process in which first $PtCl_6^{2-}$ ions are sorbed into the pores of polymer matrix followed by electroreduction at −0.55 V in a 0.5 M H_2SO_4 solution. Loading of Pt nanoparticles (10–200 μg/cm^2) onto POA matrix were accomplished by varying the concentration (2–10 mM) of the sorbate, i.e., H_2PtCl_6. The sizes of the Pt nanoparticles were determined from TEM analysis and Pt particles were found to be in the range of 10–20 nm. The crystallite phase of Pt particles in POA was examined from XRD pattern. AFM image further supports Pt particles embedded in POA matrix.

Keywords: Nanofibrillar POA; Pt nanoparticles; Electrocatalysis; TEM; XRD; AFM

1. Introduction

The fabrication of nano-sized metal particles has considerable interest in materials research due to their unique, optical, electronic, and catalytic properties [1–3] and these metal nanoparticles catalyst have been widely used for impressive applications such as catalysis, sensors and fuel cells [4–6]. Supported metal catalyst can play a crucial role for many industrially important chemical reactions. The support material enables the metal particles to be highly dispersed and stable. Various supported material such as Vulcan XC 72 [7,8], polyimide resin [9], cellulose diacetate [10] and polymer matrices [11–13] have been developed for loading metal catalyst particles and to improve the catalytic efficiency. Peng et al. [14] fabricated novel nonporous Pt network electrodes on titanium substrates through a simple hydrothermal assisted seed growth method and its active surface area was 20 times larger than polycrystalline Pt.

Currently conducting polymer matrices [15–24] have been employed as catalyst support materials for the oxidation of small organic molecules in place of conventional support because when nanoparticle catalyst is dispersed in carbon block, a part of the active sites remains inaccessible to the reactant molecules [25]. However, metal nanoparticles dispersed into conducting polymer support, not only provide access to large number of catalytic sites but also offer the possibilities of spent catalyst recovery. Lamy and co-workers [26] first studied Pt microparticles deposition on polyaniline film for methanol oxidation by electrolysis at constant potential using acidic hexachloroplatinate solutions. Different electrochemical methods such as constant potential [24], double potential step [27], potential cycling method [24] and constant current [27] have been attempted and tried for encapsulating metal nanoparticles into polymer matrices. Recently, Yamada et al. [28] synthesized PtCo alloy nanoparticles by reduction of metal coordinated nanopolymers. Majority of these techniques lead only to an agglomerated metal particles on the film and found to be less efficiency.

The main objective of the present work is to prepare controlled sizes of Pt nanoparticles in POA nanofibrillar matrix, and maintain the homogeneous distribution of Pt particles by employing a new approach. Conducting POA nanofibrillar matrices as support obtained by stepwise electro-oxidation which show enhanced electronic conductivity and transport

* Tel.: +91 4565 227550x228; fax: +91 4565 227779.
E-mail address: ccsivakumar@yahoo.com.

0013-4686/$ – see front matter © 2006 Elsevier Ltd. All rights reserved.
doi:10.1016/j.electacta.2006.11.038

properties, compared to conventionally synthesized POA. Like polyaniline, POA is also stable, can be made into dispersion in aqueous and organic media and can be cast as thin films. Loading of Pt nanoparticles in POA matrix effected by galvanostatic reduction of entrapped $PtCl_6^{2-}$ ion in the polymer matrix. These films were characterized by XRD, TEM and AFM analysis. Evaluating the various Pt nanoparticles loaded POA nanofibrillar film toward electrocatalytic applications.

2. Experimental

o-Anisidine, OA (E-Merck) was distilled under vacuum in small portions and kept under nitrogen atmosphere before use. H_2PtCl_6 (Aldrich) and Methanol (Aldrich) were used as received. All solutions were prepared with Milli-Q water. All electrochemical experiments were carried out at 25 °C using Electrochemical Analyzer model BAS 100B with a BAS electrochemical cell set-up. The working electrode was a BAS glassy carbon (GC) disk electrode (3 mm in diameter), Pt spiral wire as counter and MSE, connected with salt bridge were used reference electrodes, respectively.

2.1. Film preparation on GC electrode using cyclic voltammetry

Normal cyclic voltammetry and constant potential stepwise electro-oxidation methods were chosen for the deposition of POA film on the GC electrode. Electropolymerization of *o*-anisidine on GC electrode was carried out in 0.5 M H_2SO_4 containing 0.05 M of *o*-anisidine using potential cycling method. POA films of different thickness were obtained by varying the concentration of the monomer. The thickness of POA film on GC was determined using the charge under the first peak in the CV of redox of POA in 0.5 M H_2SO_4 [29,30] according to the procedure of Stillwell and Park.

2.2. Stepwise growth of POA film on GC

Stepwise electro-oxidation of *o*-anisidine is chosen to prepare highly ordered nanoporous film [31] on GC electrode by single potential time base (TB) galvanostatic mode [32] modified keeping in mind the electrochemical oxidation of *o*-anisidine. Briefly, a three-step method for film formation is used as described below: (a) initially, 1.0 V was applied for 60 s in order to produce a large quantity of *o*-anisidine radicals near the electrode surface; (b) followed by a step to 0.62 V for a time duration of 120 s for the interaction of radicals (oxidized dimer or oligomer) with the unreacted monomer. This potential step was selected based on the onset potential for oxidation of *o*-anisidine monomer in CV experiments; (c) finally, a potential of 0.42 V was applied for 120 s to ensure oxidation of any oligomers formed during the above potential pulse application.

2.3. Protocols for loading of Pt nanoparticles in POA matrix

Loading of Pt nanoparticles into the nanofibrillar POA matrix was performed by two-step process in which first, doping or sorption of $[PtCl_6]^{2-}$ ions by simply dipped into Pt complex solution for 1 to 2 min and allowed the polymer film to dry for 15–20 min. Next, reduction of Pt(IV) metal ions to Pt(0) metallic nanoparticles was carried out by single potential time base (TB) method that entails in applying a constant potential of −0.55 V for 100 s in 0.5 M H_2SO_4 solution. The main advantage of this method is that the metal ions are well distributed throughout the polymer matrix leading to entrapment of particles by complete reduction of the sorbed Pt complex in the porous polymer matrix. Different loading levels of Pt particles were achieved by varying the concentration of H_2PtCl_6 from 2 to 10 mM. The amount of Pt nanoparticles loaded in POA matrix was estimated by integrating the charge consumed during the electro-reduction of Pt(IV)–Pt(0) by chronoamperometry. Unreacted $PtCl_6^{2-}$ examined by UV–vis absorption spectra at 261 nm was found to be negligible indicating complete utilization of Pt salt for Pt particle deposition (figure not shown). Whereas, in cases where excess Pt salt was used intentionally for electrodeposition, the extent of unreacted $PtCl_6^{2-}$ was found to be considerable.

2.4. Characterization

The size and crystallite phase of Pt nanoparticles encapsulated in POA matrix was analyzed by PANalytical, XpertPRO, Powder X-Ray Diffractometer equipped with Cu Kα source. The size of the Pt nanoparticles in POA matrix was also investigated by TEM on Philips CM Microscope, CM200KV with a resolution of 0.23 nm using aqueous polystyrenesulphonate as dispersing agent placed on carbon-coated copper grids. Pt nanoparticles encapsulated POA films coated on BAS RDE GC electrode were characterized by PicoSPM Atomic Force Microscopy, Molecular Imaging, USA operated in contact mode. Gold-coated SiN_3 cantilever (force constant 0.12 N/m) was used as the force sensor and the radius of curvature of the probe tip was about 5–10 nm. The measurement was made with a small 6 μm piezoelectric *z*-scanner, which is standardized using calibration gratings supplied by molecular imaging. UV–vis spectrum was recorded using Perkin-Elmer 2605 UV-Visible spectrophotometer.

3. Results and discussion

3.1. Synthesis of conducting POA nanofibrillar film using stepwise electro-oxidation procedure

The present work demonstrates the generation of controlled size of Pt nanoparticles in POA conducting nanofibrillar matrix as catalyst support and electrocatalytic activity towards the electro-oxidation of methanol. For this purpose, films of POA were prepared on GC electrode using stepwise electro-oxidation procedure and the thickness of films was determined by cyclic voltammetry technique between 0.1 and 2 μm. Stepwise electro-oxidation method is found to yield good results for the formation of nanofibrillar porous POA films rather than using conventional cyclic voltammetry deposition of polymer film. A detailed procedure for preparing POA nanofibrillar film is explained in

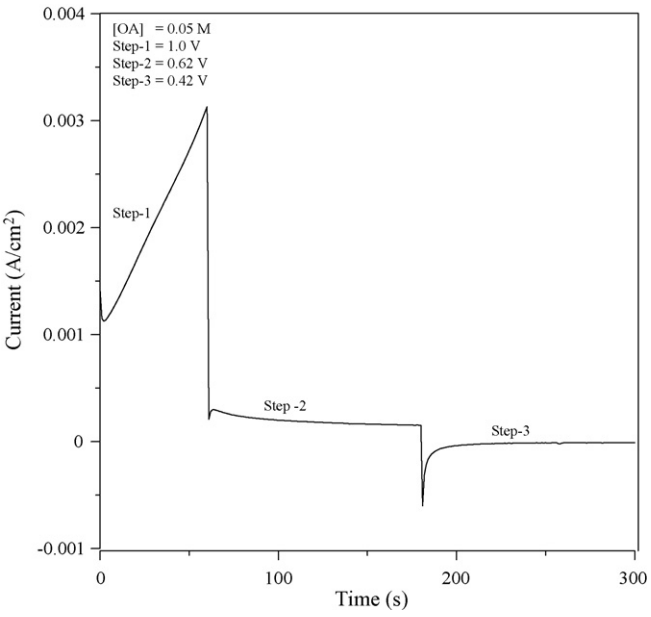

Fig. 1. The current–time behavior of POA nanofibrillar film obtained by stepwise electro-oxidation procedure.

Section 2. Fig. 1 shows the electropolymerization of *o*-anisidine by stepwise procedure. In the first step, current increased enormously after within few milliseconds. This indicates production of a large number of monomer cation radicals and starts nucleation of dimer or oligomer at the electrode surface. In the second step, linear propagation of nucleation growth with lower extent of production of oligomer radicals is possible and finally to offer nanofibrillar POA films in the third step. Scanning electron micrographs were recorded for these films and identified the formation of POA nanofibrillar films with length of 100–200 nm. Fig. 2 shows the SEM picture of POA nanofibrillar film synthesized on GC electrode as described in Section 2 with modifications to the procedure given by Lang et al. [31] and Gupta and Muira [32] and Fig. 3 shows SEM picture of Pt particles entrapped POA film obtained by (a) cyclic voltammetry technique; (b) stepwise electro-oxidation procedure. The cyclic voltammetry deposition of POA produces particulate products with small amount of nanofibers. Finally it leads to spongy or irregular morphology structure. This may be due to the secondary growth of polymer in the second and successive cycles of voltammetric deposition (Fig. 3a). But stepwise electro-oxidation procedure of *o*-anisidine is followed by three potential steps in which production of monomer radical cations, nucleation with further growth was accelerated by the monomer interaction with oxidized oligomer and finally the oxidized fibrillar morphology interconnected with each other which gives narrow orientation with almost uniform diameter (50–70 nm) of nanofibrillar morphology of POA. Here, *o*-anisidinium cations formed in the first step act as templates for the formation of nanostructured morphology. The mechanism of polymerization is fashioned with linear chain propagation by the production of a large number of radical cations in the first step and oligomers oxidized in the second step to finally form high molecular weight nanofibrillar structure. While traditional chemical or electrochemical polymerization using common mineral acids yields granular morphology of emeraldine as reported by Avlyanov et al. [33] Therefore, the SEM images of POA film prepared by stepwise electro-oxidation method are very smooth and exhibit

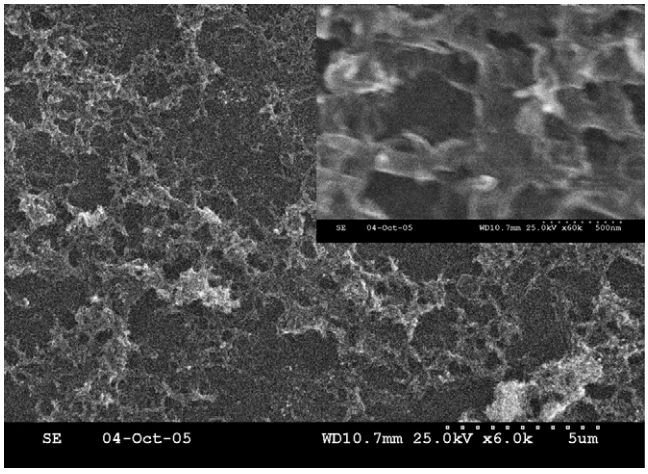

Fig. 2. SEM picture of POA nanofibrillar film synthesized via stepwise electro-oxidation procedure—low magnification: 5 μm; inset—higher magnification: 500 nm.

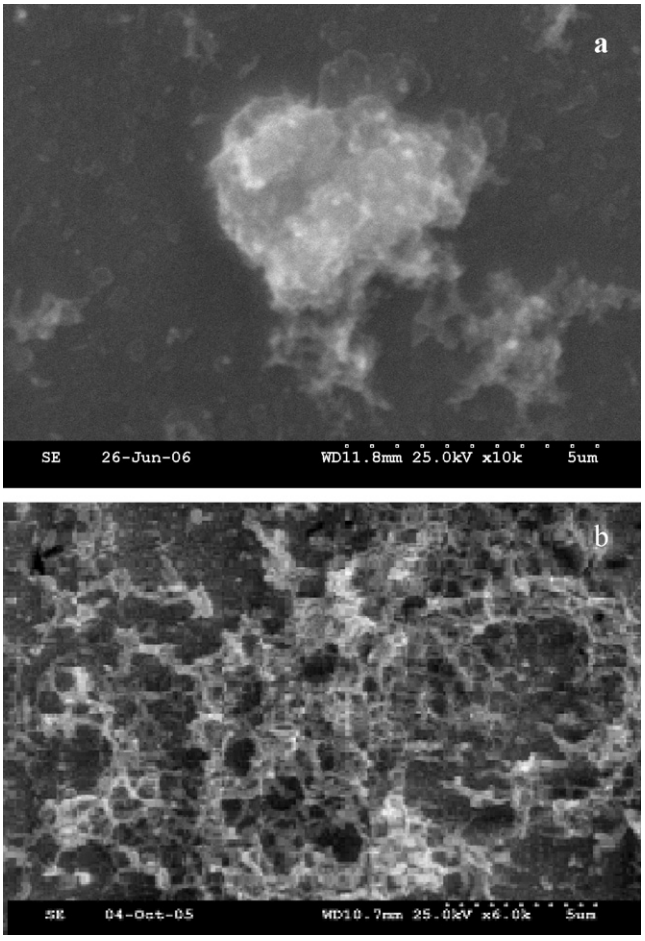

Fig. 3. SEM picture of Pt nanoparticles encapsulated POA film obtained by (a) cyclic voltammetry technique (particulate products with spongy structure); (b) stepwise electro-oxidation method—fiber length 100–200 nm.

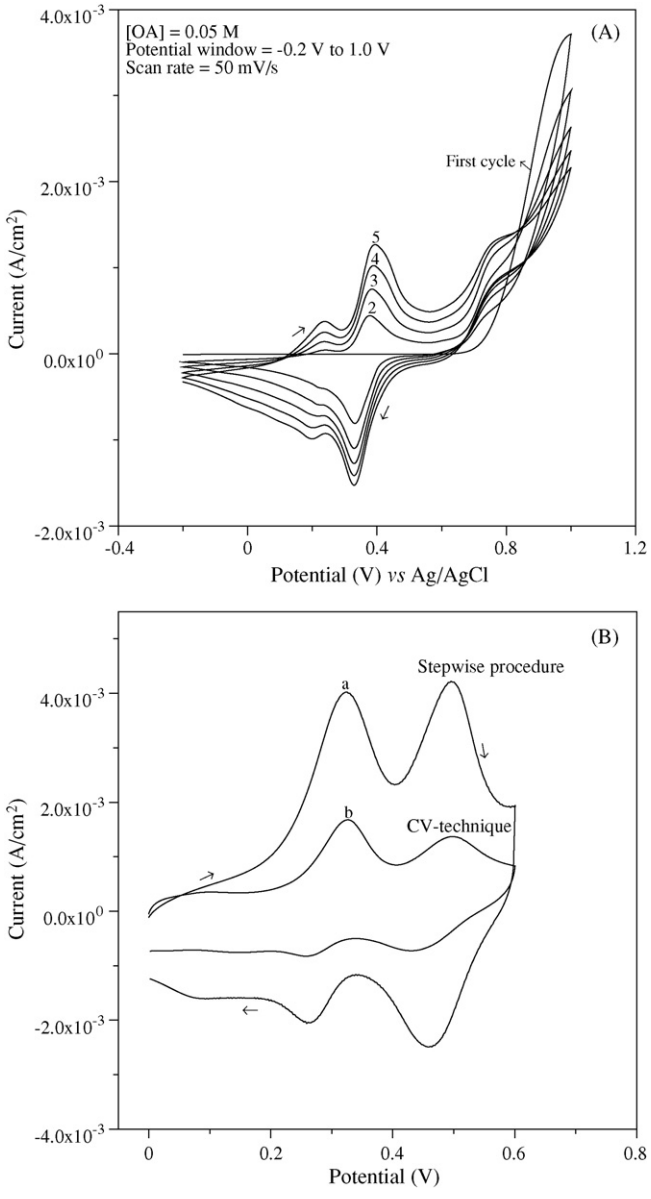

Fig. 4. (A) Cyclic voltammograms recorded for the electropolymerization of *o*-anisidine in 0.5 M H_2SO_4 in the potential range between −0.2 and 1.0 V at a scan rate of 50 mV/s. (B) Cyclic voltammogram of POA film recorded in 0.5 M H_2SO_4 at a scan rate of 50 mV/s: (a) stepwise procedure and (b) CV technique.

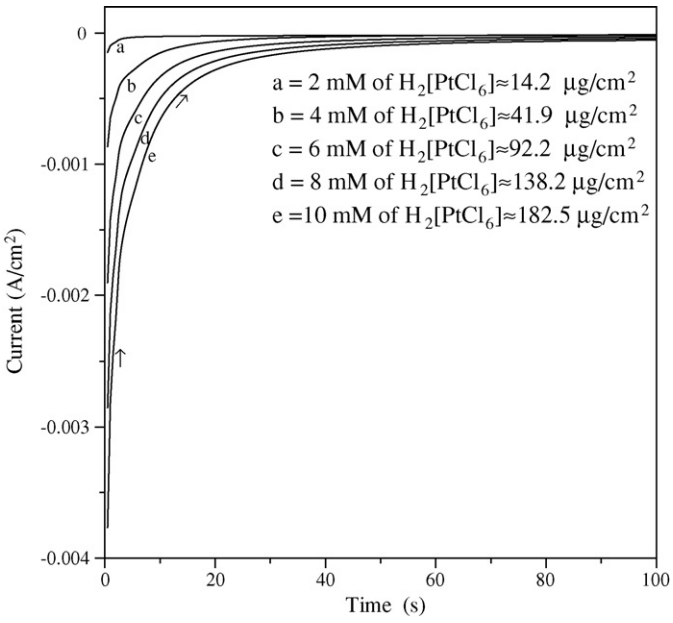

Fig. 5. Current–time behavior of reduction of Pt complex salt in POA matrix using single potential time base (TB) mode (−0.55 V vs. MSE) in 0.5 M H_2SO_4.

homogeneous nanofibrillar morphology, similar to Huang and Kaner who synthesized using interfacial polymerization route [34] and bulk synthetic method [35]. The conductivity value of POA nanofibers were in the range of 0.2–0.5 S/cm using four-probe resistivity step-up, which is approximately two times higher than that of conventionally synthesized emeraldine POA.

For comparison purpose, POA film was also prepared by cyclic voltammetry. Fig. 4A represents the cyclic voltammogram recorded for the electropolymerization of *o*-anisidine in 0.5 M H_2SO_4 for five cycles in the potential range between −0.2 and 1.0 V at a scan rate of 50 mV/s. The monomer undergoes oxidation at 0.62 V in the first cycle of CV and further scanning to 1.0 V may lead to the formation of oligomers or the polymer on GC. In the reverse scan, a peak at 0.38 V corresponds to the reduction of the oxidized oligomer. Subsequent cycles of CV indicate the POA film growth on GC with distinct two redox peaks ($E_p^a = 0.26$; 0.4 V and $E_p^c = 0.37$; 0.22 V) as evidenced by increasing peak current values. The peak potential values obtained in this study match its from reported by Patil et al. [36]. The amount of POA polymer deposited on GC was calculated by measuring the charge of first redox peak current or cathodic peak current values of CV run in the background electrolyte of 0.5 M H_2SO_4. The cyclic voltammogram of POA film modified GC electrode shows two main redox process ($E_p^a = 0.31$ V (I); 0.49 V (II) and $E_p^c = 0.46$ V (III); 0.26 V (IV)) for inter-conversion of leucoemeraldine/emeraldine and emeraldine/pernigraniline [37]. The polymer film prepared by stepwise electro-oxidation procedure has high surface area with nanofibrillar morphology and its peak current density was found to be four times higher than the films prepared by cyclic voltammetry technique (Fig. 4B). Hence, the catalyst support is an important factor for the synthesis of Pt particles for enhanced catalytic activity.

3.2. Loading of Pt nanoparticles in POA nanofibrillar matrix

Loading of Pt nanoparticles to varying extents was achieved by sorption method and explained in Section 2. Fig. 5 shows the current–time behavior of the reduction of Pt complex salt using single potential time base (TB) mode (−0.55 V versus MSE) in 0.5 M H_2SO_4 [38]. Within 10 s 90% of $[PtCl_6]^{2-}$ ions are reduced (2 mM of Pt precursor salt solution) and after that the current–time response attains steady-state. The amount of Pt nanoparticles incorporated into POA matrix was calculated by integrating the charge for the reduction of Pt(IV)–Pt(0) in TB mode and the value was found to 28.3 mC/cm^2 for using 2 mM of $H_2[PtCl_6]$ solution [29] as shown in Table 1. Like-

Table 1
Characteristics of Pt particles in POA nanofibrillar matrix and anodic peak current values of 0.5 M methanol oxidation

$[H_2PtCl_6]$ (mol l^{-1})	H_{upd} charge of Pt particles in POA from CV (mC/cm^2)	Charge consumed in converting Pt(IV)–Pt(0) in POA matrix (mC/cm^2)	Weight of Pt particles in POA (μg/cm^2)	MeOH onset potential (V) vs. MSE	Anodic peak current density values (mA/cm^2)
Bulk Pt	0.245	–	–	−0.040	0.413
0.002	0.634	28.3	14.2	−0.02	1.28
0.004	1.693	83.8	41.9	−0.073	1.92
0.006	3.558	184.3	92.2	−0.140	3.56
0.008	6.402	276.4	138.2	−0.136	2.55
0.010	7.975	364.9	182.5	−0.116	2.42

wise, 4, 6, 8 and 10 mM of Pt solutions were used for loading of 83.8, 184.3, 276.4 and 364.9 mC/cm^2, respectively. As the concentration of precursor salt increases, while keeping the sorption time constant, increases in loading of Pt particles were observed. The size of Pt particles in POA matrix can be varied by changing the concentration of metal precursor solution and identified from TEM analysis. The Pt particle sizes are in the range of 6–10 nm for using 2 mM, 10–18 nm for 4 mM, 10–30 nm for 6 mM, 50–70 nm for 8 mM and 100–200 nm for 10 mM of Pt complex salt solutions. Clearly, it shows that the Pt particle size is controlled by both the relative concentration of the metal precursor salt and polymer morphology. Hence, it is shown that this method presents an easy way of loading Pt nanoparticles into polymer matrix compared to potential cycling mode [39] or double potential step method [24].

3.3. TEM analysis of Pt nanoparticles encapsulated POA matrix

Fig. 6 shows the typical TEM image pattern obtained for Pt nanoparticles loaded POA nanofibrillar matrix and the preparative conditions described in Section 2. As can be seen from the TEM micrograph, the Pt nanoparticles are encapsulated in POA matrix with narrow size distribution. No particle aggregation was observed as evidenced from the TEM examination. The data reveals an average diameter of Pt particles to be approximately in the range between 10 and 20 nm as maximum shown in the inset of the figure for the plot of Pt particle counts versus particle size and the size of Pt nanoparticles in POA matrix strongly depends on the preparative conditions employed. In Pt_{nano}–POA film, there is a chemical interaction between POA and Pt nanoparticles in which the charge transfer takes place between amine/imine nitrogen of POA backbone and Pt particles of size 10–20 nm. The sizes of these Pt particle possess a unique electron donor–acceptor property that differs from that of bulk Pt metal as similar to Qiu et al. [40] reported the interaction of PVP polymer with pt nanoparticles. The presence of *o*-methoxy group in the POA backbone may also be enhanced the charge transfer process. Selective area of electron diffraction, SAED (Fig. 6, inset) shows a hexagonal diffraction spot pattern which indicates that the Pt(1 1 1) facets of Pt nanoparticles obtained in POA matrix. For practical applications, smaller particles have the advantage of a large specific surface area and improving the overall electrocatalytic activity of Pt nanoparticles loaded into the nanofibrillar POA matrix.

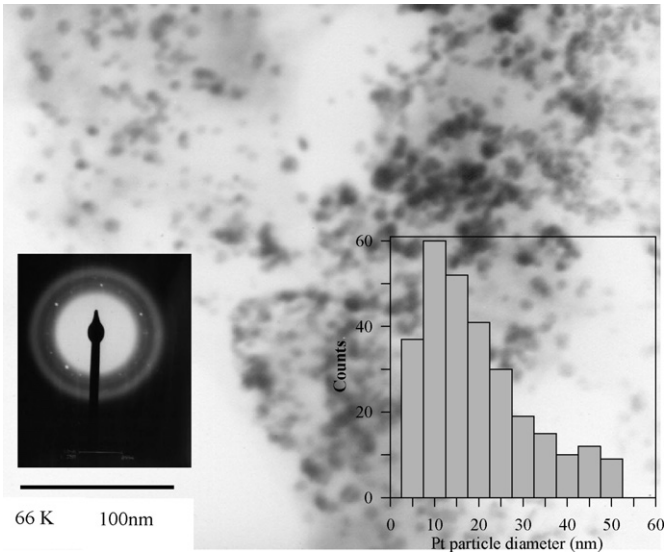

Fig. 6. TEM picture of Pt nanoparticles encapsulated POA nanofibrillar film dispersed into aqueous polystyrene sulphonate (TEM image of 100 nm magnification of Pt (92.2 μg/cm^2) nanoparticles in POA film; scale = 100 nm; 66.0 K) [inset: plot of Pt particle counts vs. particle size; SAED pattern of Pt nanoparticles in POA matrix (10 nm; 1.35 M)].

3.4. X-ray diffraction and AFM characterization of Pt nanoparticles in POA matrix

Further, XRD provides information relating to crystallite phase structure and the size of the Pt nanoparticles in nanofibrillar POA film. The characteristic diffraction pattern of 2θ values of POA film appeared at 12.8°, 22° and 30°. In addition, the Pt nanoparticles loaded into the POA film showed diffraction peaks at 39.283 for Pt(1 1 1) and 74.313 for GC, respectively (Fig. 7). Also, the 2θ position of Pt(1 1 1) diffraction peak appears to be shifted to lower values typical for a Pt(1 1 1) fcc phase of 39.7645 [41]. The XRD peaks of GC also appeared at 43.39 as predominant. The average size of the Pt particle is about 10–20 nm calculated by using Scherrer formula is in good agreement with the size obtained in the TEM analysis. Fig. 8 shows the AFM topographic image of Pt nanoparticles embedded POA film taken in contact mode using SPM scanner on GC electrode surface. Agglomerated Pt particles were seen on the surface of POA film by using 10 mM of Pt precursor salt and the particle sizes were in the range of 100–200 nm (Fig. 8). At higher

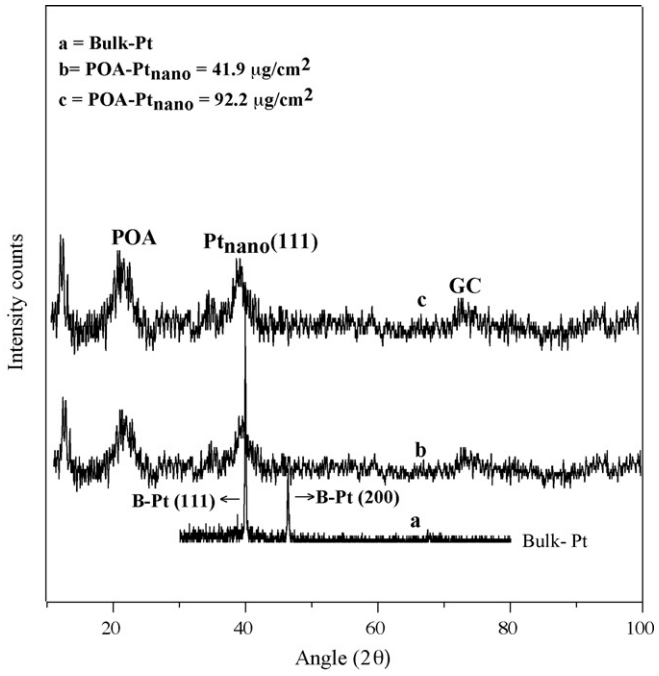

Fig. 7. XRD pattern of bulk Pt (a) and Pt nanoparticles (41.9 μg/cm^2 (b); 92.2 μg/cm^2 (c)) loaded POA nanofibrillar film.

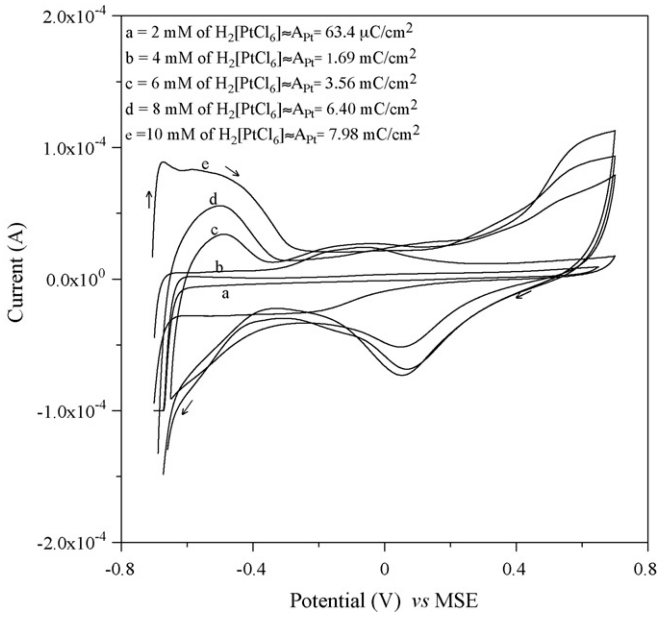

Fig. 9. Cyclic voltammogram of various amount of Pt nanoparticles loaded POA matrix recorded in 0.5 M H_2SO_4 vs. MSE. a = A_{Pt} = 63.4 μC/cm^2; b = A_{Pt} = 1.693 mC/cm^2; c = A_{Pt} = 3.56 mC/cm^2; d = A_{Pt} = 6.40 mC/cm^2; e = A_{Pt} = 7.98 mC/cm^2.

$H_2[PtCl_6]$ (≥10 mM) precursor salt solutions, only agglomerates of Pt nanoparticles were observed.

3.5. Determination of surface area of Pt nanoparticles in POA nanofibrillar matrix using H_{upd} charge

The cyclic voltammogram of Pt nanoparticles (up to H_{upd} charge of Pt loading of 3.56 mC/cm^2) entrapped POA film though did not show any hydrogen adsorption–desorption peaks exhibited peaks corresponding to platinum oxidation–reduction in 0.5 M H_2SO_4 at a scan rate of 50 mV/s versus MSE as shown in Fig. 9. The appropriate CV pattern of Pt_{nano}–POA was attained within five cycles in the background electrolyte. The charge in the H_{upd} region is a direct measure of the surface area of Pt nanoparticles in POA and presented in Table 1 for various

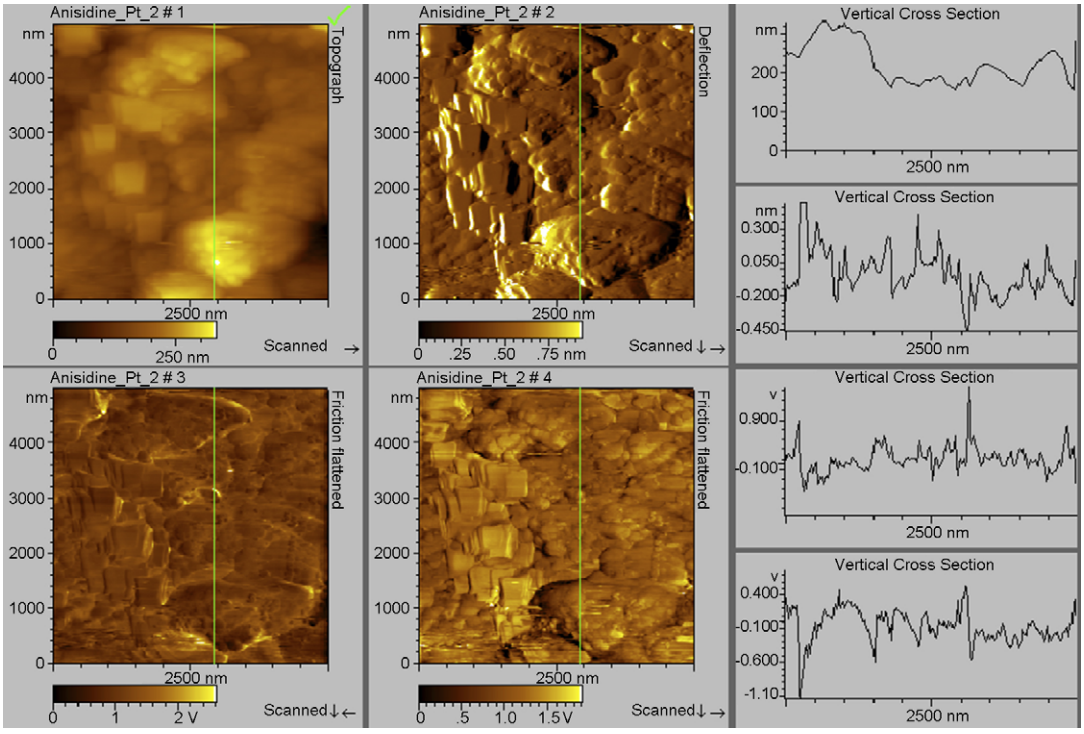

Fig. 8. AFM topographic image shows Pt nanoparticles entrapped POA matrix.

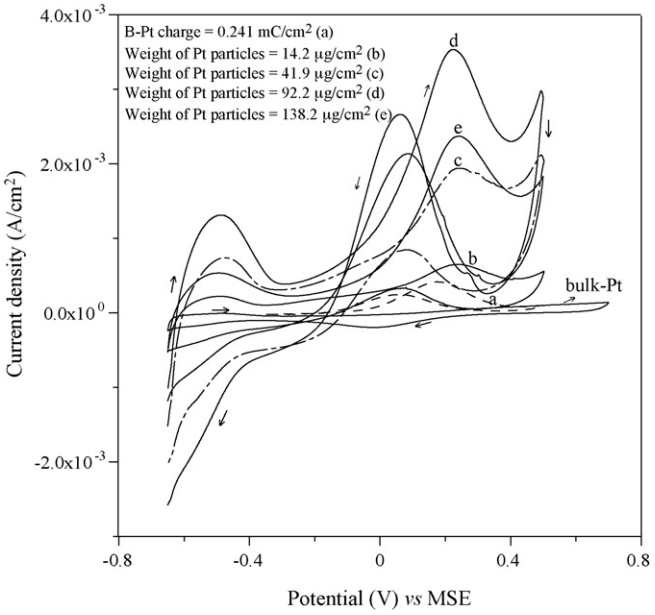

Fig. 10. Cyclic voltammograms recorded for electrocatalytic oxidation of 0.5 M methanol in 0.5 M H_2SO_4 at scan rate of 50 mV/s vs. MSE. (a) Bulk Pt; (b) 14.2 μg/cm^2 of Pt loaded in POA; (c) 41.9 μg/cm^2 of Pt loaded in POA; (d) 92.2 μg/cm^2 of Pt loaded in POA; (e) 138.2 μg/cm^2 of Pt loaded in POA.

loading levels of Pt 6 mM of Pt precursor salt solution was found suitable for loading of Pt nanoparticles (H_{upd} charge of Pt = 3.56 mC/cm^2) in POA matrix to obtain narrow size distribution with controlled particle size as evidenced from TEM picture (Fig. 6). Here, the surface area of Pt loaded POA film was found to be 17 times higher than the surface area of monolayer of hydrogen (210 μC/cm^2) of polycrystalline Pt [14].

3.6. Electrocatalytic oxidation of methanol

Cyclic voltammetry and chronoamperometry experiments were carried out for exploring the electrocatalytic behavior of Pt_{nano}–PoA towards methanol oxidation for various Pt loadings in 0.5 M H_2SO_4. Fig. 10 shows cyclic voltammograms of 0.5 M methanol oxidation at films of various Pt loadings (H_{upd} charge of 63.37 μC/cm^2 to 7.975 mC/cm^2) between −0.650 and 0.5 V at a sweep rate of 50 mV/s versus MSE in 0.5 M H_2SO_4. An anodic peak of 1.28 mA current density (charge under the peak: 63.37 μC/cm^2) appeared at 0.2 V for the POA film loaded with Pt particles. The onset of oxidation observed at −0.02 V is shifted cathodically compared to (pc) Pt, i.e., −0.04 V. Further loading of Pt particles of charge to 3.56 mC/cm^2 and the respective anodic peak current density value increases by a factor of 4 as compared with polycrystalline (pc) Pt. This may be attributed to narrow distribution of Pt particles in nanofibrillar structure of POA. Scheme 1 represents the electro-oxidation of methanol by dissociative adsorption mechanism on the surface based on [24]. The electrocatalytic activity of methanol oxidation is strongly influenced by Pt particle dispersion [14]. Here, the maximum efficiency of methanol oxidation and lower susceptibility to CO poisoning was observed due to Pt particle size between 10 and 20 nm (as evidenced from TEM picture) and

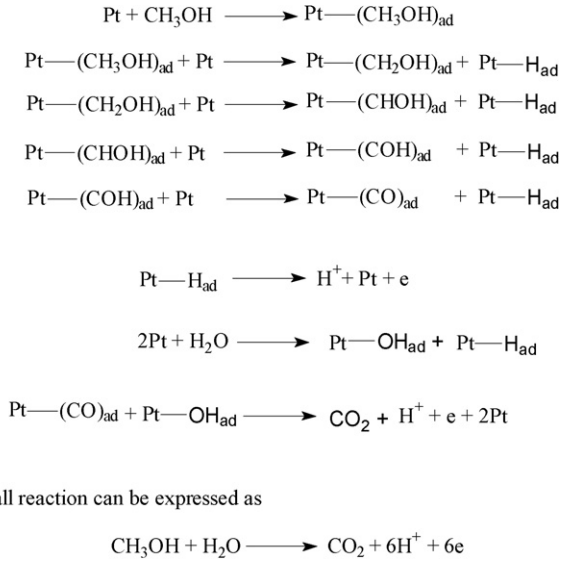

Scheme 1.

the nanofibrillar POA matrix as support. The structure of POA film synthesized by stepwise electro-oxidation procedure decorated the nanofibrillar morphology with the fiber diameter of 50–70 nm. Since the initially formed *o*-anisidinium cations act as templates for further narrow orientation of nucleation growth. This narrow orientation of nanofibrillar matrix results high surface area with uniform pore size and hence the $PtCl_6^{2-}$ ions entrapped into uniform pores of polymer matrix. Therefore, it favors the encapsulation of finely dispersed Pt particles in POA film by appropriate metal reduction. The presence of uniform pore size in the nanofibrillar morphology results the realignment of Pt nanoparticles with specific orientations like Pt(1 1 1) facets are achieved and preventing particle aggregations in the polymer matrix. These Pt(1 1 1) facets of Pt particles in POA matrix can be promoted the electrocatalytic activity of methanol oxidation because the Pt(1 1 1) phase of nanostructured Pt is more favorable for methanol oxidation with less CO poisoning. XRD results were also confirmed that the formation of Pt(1 1 1) phase of Pt nanoparticles in POA matrix. This suggests that the nanofibrillar morphology provide a crucial role in controlling the growth of Pt particles deposition. But, cyclic voltammetry deposition of POA offered spongy or irregular morphology structure with small amount of nanofibrillar matrix. Hence, the Pt salts adsorbed on the available limited pores results nonuniform or clusters of Pt particles. The main reason for the selection of this method is the formation of controlled sizes of Pt nanoparticles can be achieved by absorption of appropriate amount of $[PtCl_6]^{2-}$ ions into POA nanofibrillar matrix. The size and weight of Pt nanoparticles can also be varied easily by changing the concentration of metal precursor salt solution. A significant cathodic shift value of 100 mV onset potential was observed for loading of Pt charge of 3.56 mC/cm^2 to POA film and higher loadings, the onset potential shifted to anodic side. This observation was further confirmed from Fig. 11 represents the plot of weight of Pt particles loaded on POA matrix versus onset oxidation potential of methanol and H_{upd} charge of Pt particles loaded POA nanofibrillar matrix.

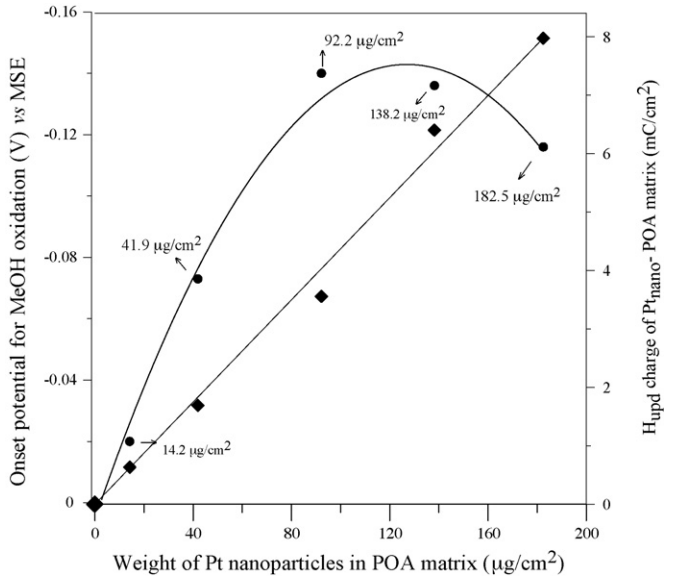

Fig. 11. Variation in onset potential of MeOH oxidation and H_{upd} charge of Pt nano in POA matrix with weight of Pt particles loaded in POA matrix.

Scheme 1 shows methanol oxidation on Pt nanoparticles encapsulated POA matrix electrode.

To further examine the stability of electrocatalytic activity of Pt_{nano}–POA film catalyst material towards methanol oxidation, chronoamperometry was performed. Fig. 12 represents the current–time behavior of POA films of various Pt loadings in 0.5 M H_2SO_4 for the electro-oxidation of 0.5 M CH_3OH at 0.2 V versus MSE for a period of 600 s. The POA–Pt catalyst prepared in the stepwise procedure shows 1.5 times higher catalytic activity than the catalyst prepared by CV technique. The current density for methanol oxidation appears around 240 μA for loading of Pt particles of charge of 3.56 mC/cm^2 in POA matrix. The current density value decreases slowly to remain at steady value after 600 s.

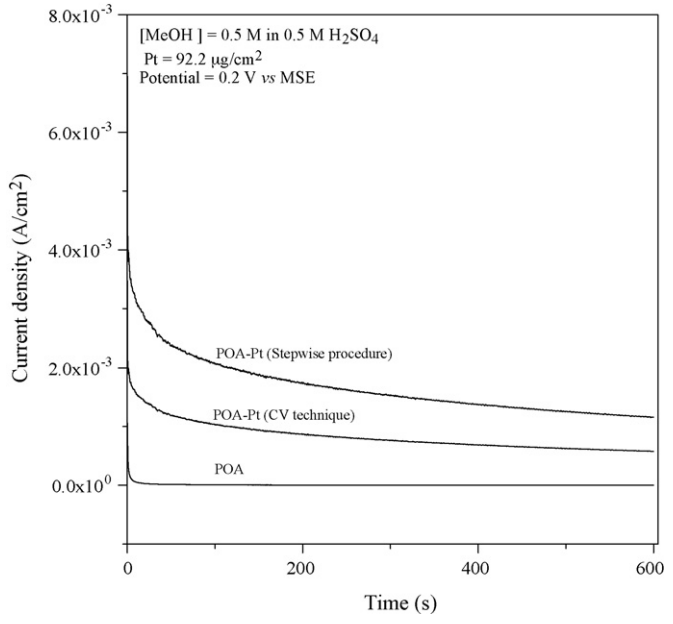

Fig. 12. The current–time behavior of various Pt loaded POA catalysts in 0.5 M H_2SO_4 for the electro-oxidation of 0.5 M CH_3OH at 0.2 V vs. MSE for a period of 600 s.

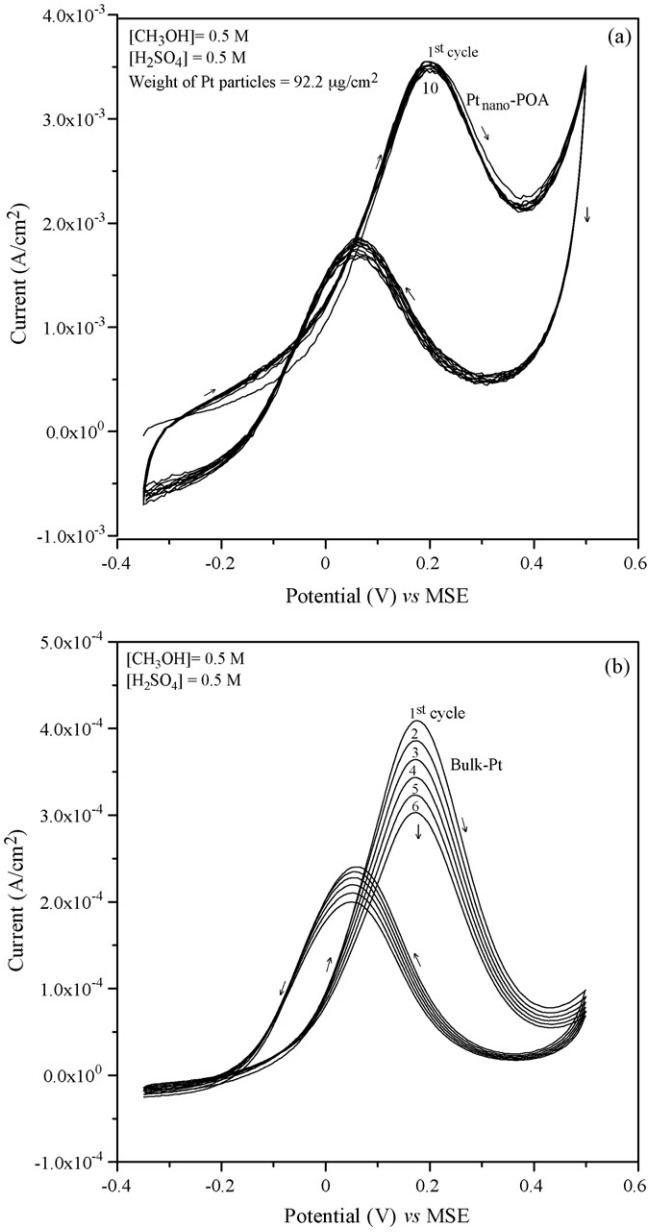

Fig. 13. Cyclic voltammogram recorded for CO poisoning effect of methanol oxidation on (a) Pt_{nano}–POA film; (b) bulk Pt in 0.5 M H_2SO_4 at a scan rate of 50 mV/s.

3.7. Comparison of CO poisoning effect of methanol oxidation on Pt_{nano}–POA film and bulk Pt

Fig. 13 shows the cyclic voltammograms recorded for CO poisoning effect of 0.5 M methanol oxidation on bulk Pt and Pt_{nano}–POA film in the potential range between −0.35 and 0.5 V versus MSE in 0.5 M H_2SO_4 at a scan rate of 50 mV/s. Methanol oxidation reaction was recorded continuously for 10 cycles to examine the CO poison effect on Pt nanoparticles encapsulated POA film and the results were compared with

bulk Pt electrode. The Faradaic current density of methanol oxidation peak was almost same or trivial variation noticed for all cycles. Because the Pt(1 1 1) facets of Pt particles in POA nanofibrillar matrix enhances the further oxidation of initially adsorbed CO to CO_2 quickly before the oxidation of methanol in the second and successive cycles. But in bulk Pt electrode, the faradic current density values of methanol oxidation have been decreased drastically with cycle number (Fig. 13b) in the same potential region. The peak current density values decreased from 0.4 to 0.3 mA/cm^2. This is due to the strong adsorption of CO molecule on electroactive surface of Pt which results decelerate in electrocatalytic activity of bulk Pt electrode. Here, a distinct difference exits between the energies of the dissociative adsorption of methanol oxidation on Pt(1 1 1) facets of Pt particles loaded POA film and bulk Pt electrode at low electrode potentials. Under these conditions bulk Pt electrode accumulates CO formation which results poisoning, but on Pt(1 1 1) CO formation requires activation by high electrode potential.

4. Conclusions

A new approach evolved for the synthesis of conducting nanofibrillar film of POA by stepwise electro-oxidation procedure and loading of Pt nanoparticles in nanofibrillar POA matrix using metal precursor salt solutions. The maximum Pt particle size values range from 10 to 20 nm, as determined from TEM analysis. The Pt nanoparticles encapsulated POA nanofibrillar film is robust, homogeneous, and have higher electrocatalytic activity because of their very high surface area (17 times higher than bulk Pt) and showed less poisoning effect than bulk Pt. The peak current density of electro-oxidation of methanol was found to be approximately 8.6 times higher than that of bulk Pt. In addition, the chronoamperometry results reveal the POA–Pt catalyst prepared in stepwise procedure shows 1.5 times higher catalytic activity than the POA–Pt catalyst prepared by potential cycling method. This enhanced rate of electrocatalytic activity may be due to finely dispersed Pt nanoparticles in POA nanofibrillar matrix and attributed to POA encapsulation of Pt nanoparticles. The major portion of Pt nanoparticles in POA nanofibers matrix was identified from XRD pattern as Pt(1 1 1) crystalline phase. SEM images show that POA film growth leads to nanofibrillar structure during the stepwise electro-oxidation. AFM results also show great extent of roughness of the Pt nanoparticles entrapped POA matrix.

Acknowledgements

The author is gratefully acknowledged the financial support from CSIR, New Delhi for Research Associateship work. K.L.N. Phani is gratefully acknowledged for helpful discussions and J. Mathiayarasu for skilled help in acquiring AFM images.

References

[1] M. Antonietti, C. Goltner, Angew. Chem. Int. Ed. 36 (1997) 90.
[2] G. Sohmid, L.F. Chi, Adv. Mater. 10 (1998) 515.
[3] A.P. Alivisatos, Science 271 (1996) 993.
[4] G.L. Cho, B.B. Lakshmi, E.R. Fisher, C.R. Martin, Nature 393 (1998) 46.
[5] J. Pei, X.Y. Li, J. Electroanal. Chem. 441 (1998) 225.
[6] H. Bonnemamn, N. Waldofner, Chem. Mater. 14 (2002) 1115.
[7] I.S. Armadi, Z.L. Wang, T.C. Green, A. Henglein, M.A. El-Sayed, Science 272 (1996) 1924.
[8] B. Legratiet, H. Remita, G. Picq, M.O. Delcourt, J. Catal. 164 (1996) 36.
[9] (a) K. Akamatsu, S. Ikeda, H. Nawafune, S. Deki, Chem. Mater. 15 (2003) 2488;
(b) K. Akamatsu, H. Sinkai, S. Ikeda, S. Adachi, H. Nawafune, S. Tomita, J. Am. Chem. Soc. 127 (2005) 7980.
[10] Y. Huang, D. Li, P. He, C. Sun, M. Wang, J. Li, J. Electroanal. Chem. 579 (2005) 277.
[11] H. Jocowitz, M. Li, D.R. Baer, M.H. Engelhard, J. Janata, J. Electrochem. Soc. 142 (1995) 798.
[12] A. Sargent, T. Loi, S. Gal, O.A. Sadik, J. Electroanal. Chem. 470 (1999) 144.
[13] (a) M.J. Croissant, T. Napporn, J.M. Leger, C. Lamy, Electrochim. Acta 43 (1998) 2447;
(b) Y. Zhou, H. Itoh, T. Uemura, K. Naka, Y. Chujo, Langmuir 18 (2002) 277.
[14] X. Peng, K. Koczkur, S. Nigro, A. Chen, Chem. Commun. (2004) 2872.
[15] A.A. Mikhylova, E.B. Molodkina, O.A. Khazova, J. Electroanal. Chem. 509 (2001) 119.
[16] C. Coutanceau, M.J. Croissant, T. Napporn, C. Lamy, Electrochim. Acta 46 (2000) 579.
[17] H. Laborde, J.M. Leger, C. Lamy, J. Appl. Electrochem. 24 (1994) 219.
[18] L. Niu, Q.H. Li, F.H. Wei, X. Chen, H. Wang, J. Electroanal. Chem. 544 (2003) 121.
[19] M. Hepel, J. Electrochem. Soc. 145 (1) (1998) 124.
[20] Z. Qi, P.G. Pickup, Chem. Commun. (1998) 15.
[21] S. Biallozar, A. Kupniewska, V. Jasulaitene, Fuel Cells 3 (1–2) (2003) 8.
[22] A.P. O'Mullane, S.E. Dale, J.V. Macpherson, P.R. Unwin, Chem. Commun. (2004) 1606.
[23] L. Niu, Q. Li, F. Wei, X. Chen, H. Wang, Synth. Met. 139 (2003) 271.
[24] L. Niu, Q. Li, F. Wei, S. Wu, P. Liu, X. Cao, J. Electroanal. Chem. 578 (2005) 331.
[25] F. Bensebaa, A.A. Farah, D. Wang, C. Bock, X. Du, J. Kung, Y.L. Page, J. Phys. Chem. B 109 (2005) 15339.
[26] H. Laborde, J.M. Leeger, C. Lamy, J. Appl. Electrochem. 24 (1994) 219.
[27] K. Bouzek, K.M. Mangold, K. Jutter, Electrochim. Acta 46 (2000) 661.
[28] M. Yamada, M. Maesaka, M. Kurihara, M. Sakamoto, M. Miyake, Chem. Commun. (2005) 4851.
[29] D.E. Stilwell, S.M. Park, J. Electrochem. Soc. 145 (1998) 124.
[30] D.E. Stilwell, S.M. Park, J. Electrochem. Soc. 135 (1988) 2491.
[31] L. Lang, J. Liu, C.F. Windisch Jr., G.J. Exarhos, Y. Lin, Angew. Chem. 114 (19) (2002) 3817.
[32] V. Gupta, N. Muira, Electrochem. Commun. 7 (2005) 995.
[33] J.K. Avlyanov, J.Y. Josefowicz, A.G. MacDiarmid, Synth. Met. 73 (1995) 205.
[34] J. Huang, R.B. Kaner, J. Am. Chem. Soc. 126 (2004) 851.
[35] J. Huang, S. Virji, B.H. Weiller, R.B. Kaner, Chem.-Eur. J. 10 (2004) 1314.
[36] S. Patil, M.A. More, P.P. Patil, J. Appl. Polym. Sci. 74 (1999) 3009.
[37] L.H. Mascaro, D. Goncalves, L.O.S. Bulhoes, Thin Solid Films 461 (2004) 243.
[38] J.M. Elliott, G.S. Attard, P.N. Bartlett, N.R.B. Coleman, D.A.S. Merckel, J.R. Owen, Chem. Mater. 11 (1999) 3602.
[39] H. Yang, T.H. Lu, K. Xue, S.G. Sun, G.Q. Lu, S.P. Chen, J. Electrochem. Soc. 144 (1997) 2302.
[40] L. Qiu, F. Liu, L. Zhao, W. Yang, J. Yao, Langmuir 22 (2006) 4480.
[41] C. Bock, C. Paquet, M. Couillard, G.A. Botton, B.R. MacDougal, J. Am. Chem. Soc. 126 (2004) 8028.